Clinical Radiology 74 (2019) 178–186

Contents lists available at ScienceDirect

Clinical Radiology

journal homepage: www.clinicalradiologyonline.net

Relationship between ^{18}F-FDG PET metabolic parameters and MRI intravoxel incoherent motion (IVIM) histogram parameters and their correlations with clinicopathological features of cervical cancer: evidence from integrated PET/MRI

S. Du [a,b], H. Sun [a,b,*], S. Gao [a,b], J. Xin [a], Z. Lu [a,b], Z. Chen [c], S. Pan [a], Q. Guo [a]

[a] *Department of Radiology, Shengjing Hospital of China Medical University, Sanhao Street No36, Heping District, Shenyang, Liaoning 110004, China*

[b] *Liaoning Provincial Key Laboratory of Medical Imaging, Sanhao Street No36, Heping District, Shenyang, Liaoning 110004, PR China*

[c] *GE Healthcare, Beijing, 100176, PR China*

ARTICLE INFORMATION

Article history:
Received 12 June 2018
Accepted 9 November 2018

AIM: To explore the relationship between positron-emission tomography (PET) and intravoxel incoherent motion (IVIM) histogram parameters and their correlations with the clinicopathological features of cervical squamous cell cancer (CSCC).

MATERIALS AND METHODS: Forty-four patients with CSCC underwent pelvic combined PET/magnetic resonance imaging (MRI) including IVIM sequences. The maximum/mean standardized uptake value (SUV_{max}/SUV_{mean}), metabolic tumour volume (MTV), and total lesion glycolysis (TLG) of PET, histogram parameters of apparent diffusion coefficient (ADC), IVIM biomarkers of tissue diffusivity (D), and perfusion fraction (F) were calculated. Correlations between SUV and IVIM (including ADC) histogram parameters, imaging parameters and clinicopathological features were evaluated.

RESULTS: SUV showed weak or no correlations with most histogram parameters of ADC, D, and F, except for a moderate correlation between SUV_{max} or SUV_{mean} and ADC_{min} (r=−0.69, p<0.001; r=-0.66, p=0.005). MTV, TLG were significantly higher (p<0.05) in tumours with larger diameters, advanced stages, and higher squamous cell carcinoma antigen (SCC-ag). SkewnessADC, kurtosisADC, entropyADC, and kurtosisD for tumour diameters, skewnessF and kurtosisF for tumour stages, kurtosisADC and entropyADC for SCC-ag were statistically significant (p<0.05). MTV (p=0.003), TLG (p=0.004), P10ADC (p=0.001), P25ADC (p=0.021), P10D (p<0.001) and P75F (p=0.014) were significantly different between G1/2 and G3 tumours. The receiver operating characteristic (ROC) curve indicated that P10D had the largest area under curve (AUC=0.868).

* Guarantor and correspondent: H. Sun, Department of Radiology, Shengjing Hospital of China Medical University, Shenyang, Liaoning 110004, PR China. Tel.: +86 24 96615 73258; fax: +86 24 23929902.
E-mail address: sunhongzan@126.com (H. Sun).

https://doi.org/10.1016/j.crad.2018.11.003

CONCLUSION: No universal correlations between SUV and IVIM parameters were found in this study, and further investigation of PET and IVIM parameters as independent potential biomarkers should be investigated for evaluating the clinicopathological characteristics of cervical cancer.

Introduction

Cervical cancer is the third most common malignancy of the female reproductive system and the fourth most common cause of cancer deaths in women worldwide.[1] A reliable diagnosis of primary cervical cancer is of great significance for developing a treatment plan and for predicting prognoses. Positron-emission tomography (PET) and diffusion-weighted (DW) magnetic resonance imaging (MRI) are amongst the most frequently used functional imaging technique for tumour diagnosis, staging, follow-up and therapeutic evaluation. PET has become part of the work-up for detecting the primary tumour and metastatic disease. Maximum standardized uptake (SUV_{max}) was considered valuable for predicting lymph node metastasis and was found to be an independent predictor of cervical cancer recurrence and prognoses evaluation.[2,3] Although volume-based PET metabolic parameters (metabolic tumour volume (MTV) and total lesion glycolysis (TLG) are not routinely measured, the prognostic value and influencing factors of MTV and TLG have been identified in numerous cervical cancer studies.[4–6] The MTV and TLG of cervical squamous cell cancer (CSCC) were found correlate with squamous cell cancer antigen (SCC-ag) levels, the International Federation of Gynaecology and Obstetrics (FIGO) stage, maximum tumour diameters, and cervical stromal invasion depth.[4] Tumours with higher MTV and TLG are more likely to demonstrate lymph node metastasis and poorer prognoses.[5,6]

DW-MRI is a functional imaging method that reflects the Brownian motion of water molecules. The apparent diffusion coefficient (ADC), a product of DWI, can provide information about tumour invasiveness, subtype characteristics, and treatment response.[7–9] Based on DWI theory, other imaging methods have emerged, such as the intravoxel incoherent motion (IVIM) theory.[10] According to the IVIM model, both pure extravascular molecular diffusion and microcirculation of blood within the capillaries (perfusion) can be separated using a bi-exponential decay function, providing additional parameters for tissue characterization.[10] IVIM parameters have a value equal to or even higher than that of ADC in evaluating tumour subtypes and grades[11] and have great potential for predicting early treatment responses and prognoses.[12,13] In addition to improved imaging methods, the acquisition methods of imaging data are also an important part of accurately assessing tumour characteristics. Previous studies[3,7–9,12–14] of DWI and IVIM mostly used region of interest (ROI)-based analysis, that is, selecting the main levels of lesions and calculating the average values; however, the parameters obtained were highly susceptible to the subjective influence of the measurers. Histogram analysis, which evaluates the frequency distribution of signal intensity or parameters, has become a promising method for characterizing tumour biology in recent years. Histogram analysis applied to ADC maps can provide more meaningful parameters, such as percentiles and heterogeneity parameters (skewness, kurtosis, and entropy), as reported by Downey *et al.*[15] It is generally based on volumetric methods, that is, voxels of the entire lesion are included in the volume of interest (VOI), so the parameters are no longer affected by the location or number of the ROI, allowing a more complete assessment of the entire lesion and thereby increasing the sensitivity and repeatability of the measurement.[16] Many studies have confirmed the importance of ADC histogram parameters in evaluating cervical cancer,[15,17,18] but the combination of the IVIM model and histogram analysis has rarely been applied to cervical cancer.

PET and IVIM imaging are based on different principles that reflect tumour metabolism, water diffusion, and microcirculatory perfusion. Many studies have attempted to find the relationship between SUV and ADC[3,19–23] as well as between imaging parameters and clinicopathological features,[3,14,23] but the results are still controversial. Recently, the introduction of integrated PET/MRI has enabled the simultaneous scanning and registration of PET and MRI data to improve data accuracy for comparisons between the two techniques. Therefore, the aim of the present study was to find the possible relationship between PET parameters and IVIM histogram parameters and their correlations with clinicopathological features of CSCC.

Materials and methods

Participants

Sixty-eight patients with cervical cancer were initially recruited from May 2017 to March 2018. The study was approved by the local institutional review board and all patients provided written informed consent. These patients underwent PET/CT examinations followed by pelvic PET/MRI (interval 90.8±12.4 min). The inclusion criteria were the following: biopsy results of CSCC were confirmed and no intrauterine device implantations; no treatment had been performed before PET/MR examinations; hypermetabolism was detected in the cervix on PET images; the

maximum diameter of the tumour was at least 2 cm on axial T2-weighted imaging (T2WI); and the PET and IVIM images were of good quality. Finally, 44 patients (median age 55 years) met all of the above criteria for participation in the image processing and analysis.

Data acquisition

The PET/MRI examinations were acquired using a GE Signa PET/MRI system (Signa, GE Healthcare, Waukesha, WI, USA), which consisted of an integrated system, combining time-of-flight PET and a 3 T MRI scanner (GE Signa 750w), with PET and MRI data being collected simultaneously. Patients fasted 4–6 hours before the PET/CT examinations to ensure that the blood glucose levels were <11.1 mmol/l. A total of 4 MBq/kg of 2-[^{18}F]-fluoro-2-deoxy-D-glucose (^{18}F-FDG) was injected via the cubital vein under calm conditions. Pelvic PET/MRI was performed 110–135 minutes (122.8±20.2 minutes) after the ^{18}F-FDG injection. A 32-channel coil (upper anterior array) was applied, and the scan sequence consisted of a sagittal T2-weighted fat suppression propeller sequence (repetition time/echo time [TR/TE] = 4,323/65 ms, section thickness/gap=6/1.2 mm, field of view [FOV] = 24 cm, matrix size = 384×384, and number of excitation [NEX] = 4); an axial T2 propeller sequence (TR/TE = 498/79 ms, section thickness/gap=6/2 mm, FOV = 36 cm, matrix size = 384×384, and NEX = 1.5); an axial T1-weighted fast spin-echo (FSE) sequence (TR/TE = 500/8 ms, section thickness/gap=6/2 mm, FOV = 26 cm, matrix size = 384×384, and NEX = 2). and an axial DWI sequence (TR/TE = 4,000/238 ms, matrix = 128×128, FOV = 40 cm, slice thickness/gap=6/2 mm, and NEX=6) with two b-values of 0 and 800 s/mm2. The IVIM sequence was performed with the following imaging parameters: TR= 6,900 ms/minimum TE, matrix = 128×128, FOV = 40 cm, section thickness/gap=6/2 mm, NEX = 6, and b-values = 0, 10, 25, 50, 75, 100, 125, 150, 200, 300, 400, 600, 800, and 1,000 s/mm2.

The two-point Dixon MRI sequence was used to perform attenuation correction of gamma rays during PET. Images were reconstructed using the three-dimensional (3D) iterative ordered-subset expectation maximization (OSEM) algorithm, three iterations and 28 subsets, a 4-mm full width at half maximum (FWHM) Gaussian filter and a 128×128 image matrix. The PET and MRI were performed in isocentres, with the same scan volumes to ensure optimal time and anatomical alignment. The total pelvic PET/MRI scanning time was approximately 15 minutes.

Imaging analysis

The images acquired from the PET/MRI examination were imported into Advantage Workstation 4.6 (GE Medical System, Milwaukee, WI, USA). Fused-PET/MR software was used for PET/MRI image analysis. The VOI was placed on each PET tumour site (SUV_{max} threshold 42%), and the inclusion of the physiological ^{18}F-FDG uptake was avoided. The following parameters were recorded: SUV_{max} (the highest SUV within the tumour VOI), MTV (the sum of the volumes of all voxels greater than 42% SUV_{max}), and TLG (SUV_{mean} multiplied by MTV). The FuncTool software was used for DWI and IVIM image post-processing, which provided the ADC, D, F, and D* metrics mapped on a pixel-by-pixel basis. The relationship between the mono-exponential and bi-exponential model signal change and the b values were expressed as follows:

$S/S_0 = -\exp(b\times ADC)$; $S(b)/S(0) = F\times\exp[-b\times(D^*+D)]+(1-F)\times\exp-(b\times D)$[10], where D is the slow diffusion coefficient, which represents the diffusion motion of pure water molecules, D* is the fast diffusion coefficient, which represents the microcirculatory perfusion, and F is the perfusion-related diffusion fraction, which represents the fractional volume occupied in voxels by flowing spins.

After browsing post-processing images of each patient, ADC, D, and F maps (Fig 1c, e, g) were processed off-line using GE's AK (Artificial Intelligent Kit) software. The contoured ROI was manually delineated along the edge of the lesions on ADC maps, while referencing T2WI and excluding the first and last layer in order to avoid partial volume effect. In order to ensure same exclusion area (haemorrhagic/cystic/necrotic tumour components or the endocervical canal) and amend subtle misregistrations (due to bladder filling during the examination) between PET images and ADC maps, manual adjustments needed to be performed to guarantee an optimal ROI location. Then, the AK software can automatically generate 3D ROIs based on axial images to improve the accuracy of ROI contouring. Additionally, ROIs on ADC maps can be directly copied to D and F maps.

All measures were performed in consensus by two radiologists with 10 and 15 years of experience in gynaecological tumour imaging diagnosis. They were blinded to the clinicopathological results. Histograms of ADC, D, and F maps (Fig 1d, f, h) were acquired, and the following parameters were estimated: the minimum (min), maximum (max), median (med), and mean; the 10th (P10), 25th (P25), 75th (P75), and 90th (P90) percentiles; and histogram heterogeneity parameters (skewness, kurtosis, and entropy). Let X denote the three dimensional image matrix with N voxels and p the first order histogram divided by N_l discrete intensity levels. Skewness represents the degree of asymmetric distribution in the histogram. High values of skewness means that the distribution is asymmetric otherwise the image is more symmetric; negative skewness means that the data areon the left side of the mean and less on the right side and the visual representation is that the left tail is longer than the right tail, the opposite is referred as positive skewness. Skewness can be defined as: $skewness = \frac{\frac{1}{N}\sum_{i=1}^{N}(X(i)-\overline{X})3}{\left(\sqrt{\frac{1}{N}\sum_{i=1}^{N}(X(i)-\overline{X})2}\right)3}$. Kurtosis is a measure of whether the data are heavy-tailed or light-tailed relative to a normal distribution. That is, histogram with high kurtosis tend to have heavy tails, or outliers. Data sets with low kurtosis tend to have light tails, or lack of outliers. Usually the size of positive and negative kurtosis is compared with the normal distribution curve. Positive kurtosis indicates the distribution is more precipitous than the normal distribution. The negative kurtosis indicates that the

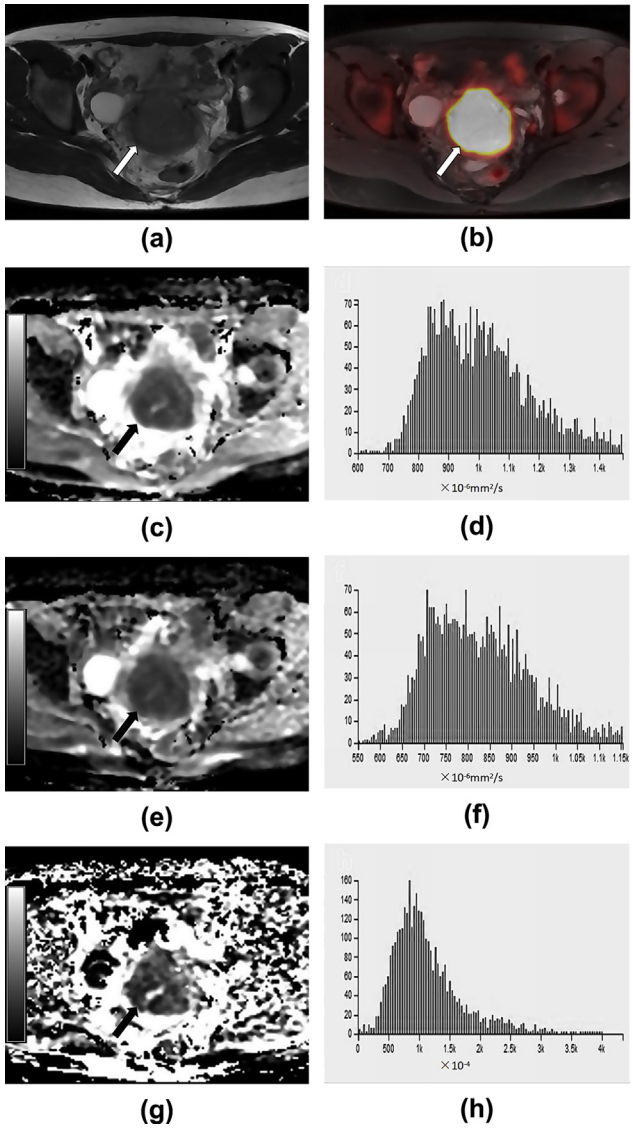

PET parameters		D_{med} ($\times10^{-6}mm^2/s$)	819.65
SUV_{max}	25.10	P10D ($\times10^{-6}mm^2/s$)	592.28
SUV_{mean}	15.76	P25D ($\times10^{-6}mm^2/s$)	738.78
MTV (ml)	74.12	P50D ($\times10^{-6}mm^2/s$)	818.50
TLG (g)	1168.13	P75D ($\times10^{-6}mm^2/s$)	912.72
ADC histogram parameters		P90D ($\times10^{-6}mm^2/s$)	1013.94
ADC_{min} ($\times10^{-6}mm^2/s$)	572.00	SkewnessD	1.46
ADC_{max} ($\times10^{-6}mm^2/s$)	2258.00	KurtosisD	3.80
ADC_{mean} ($\times10^{-6}mm^2/s$)	1040.19	EntropyD	6.70
ADC_{med} ($\times10^{-6}mm^2/s$)	994.53	F histogram parameters	
P10ADC ($\times10^{-6}mm^2/s$)	618.28	F_{min} ($\times10^{-4}$)	0
P25ADC ($\times10^{-6}mm^2/s$)	882.46	F_{max} ($\times10^{-4}$)	10000
P50ADC ($\times10^{-6}mm^2/s$)	997.83	F_{mean} ($\times10^{-4}$)	1167.04
P75ADC ($\times10^{-6}mm^2/s$)	1128.93	F_{med} ($\times10^{-4}$)	996.09
P90ADC ($\times10^{-6}mm^2/s$)	1320.76	P10F ($\times10^{-4}$)	544.15
SkewnessADC	1.52	P25F ($\times10^{-4}$)	790.63
KurtosisADC	3.25	P50F ($\times10^{-4}$)	1005.94
EntropyADC	6.66	P75F ($\times10^{-4}$)	1890.02
D histogram parameters		P90F ($\times10^{-4}$)	1962.19
D_{min} ($\times10^{-6}mm^2/s$)	534.00	SkewnessF	4.57
D_{max} ($\times10^{-6}mm^2/s$)	1784.00	KurtosisF	42.79
D_{mean} ($\times10^{-6}mm^2/s$)	842.91	EntropyF	5.74

Figure 1 Imaging findings in a patient with a histopathologically confirmed G2 cervical squamous cell cancer in FIGO stage IIb. Simultaneous acquisition of axial T2WI (a), ^{18}F-FDG PET, and T2WI fusion images (b) displayed in the cervix. (c–d) ADC map of the tumour and ADC histogram. (e–f) D map of the tumour and D histogram. (g–h) F map of the tumour and F histogram. The results of each parameter is shown (i). SUV, standardized uptake value, MTV, metabolic tumour volume, TLG, total lesion glycolysis, ADC, apparent diffusion coefficient, D, slow diffusion coefficient, F, perfusion-related diffusion fraction, PnADC, the nth percentile of ADC, PnD, the nth percentile of D, PnF, the nth percentile of F.

distribution is smoother than the normal distribution. Kurtosis can be defined as: $kurtosis = \frac{\frac{1}{N}\sum_{i=1}^{N}(X(i)-\overline{X})4}{\left(\sqrt{\frac{1}{N}\sum_{i=1}^{N}(X(i)-\overline{X})2}\right)2}$. Entropy measures the randomness of a distribution of coefficient values over the intensity levels. A simple image has low entropy, while a complex image has high entropy. Entropy can be defined as: $entropy = -\sum_{i=1}^{Nl} p(i)\log_2 p(i)$.

Clinicopathological features analysis

The maximum diameters of CSCC were measured on axial T2WI showing the largest area in reference to the other MRI sequences. The individual measurements of the two radiologists were averaged to obtain the final result. SCC-ag assays were carried out by radioimmunoassay prior to any treatment. The upper limit of normal values was 1.5 ng/ml. Patients included in the study were confirmed FIGO stage Ib–IVb via gynaecological examinations. The tumour grades of the 17 patients treated in the surgery group were based on the postoperative pathology reports. For the 27 patients in the concurrent chemoradiation and palliative chemotherapy groups, the pretreatment biopsy results were referenced.

Statistical analysis

Statistical analyses were performed using the SPSS 22.0 software (IBM, Chicago, IL, USA). Medians and ranges were used for continuous variables. To assess the relationships

between imaging parameters and clinicopathological variables, these data were dichotomous. The patients were divided into those in FIGO stage IIa or below and those in FIGO stage IIb or above. Additionally, patients were grouped into those with axial diameters <4 and ≥4 cm, and serum SCC-ag levels were divided into relatively high and relatively low groups with the cut-off of the median. Finally, the participants were grouped based on tumour grade (G1/2 and G3) according to the postoperative pathology reports or the biopsy results. Spearman's tests were used to analyse the correlations between SUV and histogram parameters of ADC, D, and F. $|r| > 0.8$ indicated strong correlations, $|r| < 0.5$ indicated weak correlations, and other values indicated moderate correlations. Mann–Whitney *U*-tests were used to compare the subgroups. Receiver operator characteristic (ROC) curve analysis was used to determine the sensitivity and specificity of the cut-off values for the separation. $p<0.05$ was considered statistically significant.

Results

CSCC presented as hypermetabolic masses on PET images, hyperintensities on T2WI, and as inhomogeneous high signal compared with normal cervical tissue on IVIM images. The clinicopathological characteristics of all 44 patients are summarized in Table 1. The PET and IVIM histogram parameters are shown in Table 2.

Correlational analysis

Correlations between SUV and histogram parameters of ADC, D, and F are shown in Fig 2. There are only very weak correlations or no correlations, except for a moderately significant negative correlation between SUV_{max} or SUV_{mean} and ADC_{min} ($r=-0.69$, $p<0.001$; $r=-0.66$, $p=0.005$, respectively). The correlation coefficients between SUV and the other ADC histogram parameters ranged between −0.30 to −0.42, and those of SUV and D histogram parameters ranged between −0.33 and −0.48.

Table 1
Clinicopathological characteristics.

Clinicopathological characteristics	Value
No. of patients	44
Patient age, median (range)	55 (30–75 years)
Tumour diameters, median (range)	3.72 (2.47–8.85 cm)
SCC-ag, median (range)	4.0 (0.8–70 ng/ml)
Pathology	
Squamous cell cancer	44 (100%)
Tumour diameter, *n* (%)	
<4 cm	20 (45.45%)
≥4 cm	24 (54.55%)
FIGO stage, n (%)	
Ib	10 (22.73%)
IIa	7 (15.91%)
IIb	10 (22.73%)
IIIb	15 (34.10%)
IVb	2 (4.55%)
SCC-ag, *n* (%)	
<4 ng/ml	22 (50%)
≥4 ng/ml	22 (50%)
Histologic differentiation (grade), *n* (%)	
Well–moderately (G1/2)	31 (70.45%)
Poor (G3)	13 (29.55%)

FIGO, International Federation of Gynaecology and Obstetrics, SCC-ag, squamous cell carcinoma antigen.

Table 2
Positron-emission tomography (PET) parameters and histogram parameters of ADC, D, and F of the 44 patients with cervical squamous cell cancer.

Parameter	Median (range)
PET parameters	
SUV_{max}	19.37 (7.87–42.77)
SUV_{mean}	12.62 (5.03–28.26)
MTV (ml)	16.41 (3.58–104.00)
TLG(g)	212.43 (20.23–2127.84)
ADC histogram parameters	
ADC_{min} ($\times10^{-6}$ mm^2/s)	546.50 (106.00–868.00)
ADC_{max} ($\times10^{-6}$ mm^2/s)	2257.00 (1549.60–3041.01)
ADC_{mean} ($\times10^{-6}$ mm^2/s)	1107.88 (777.42–1395.04)
ADC_{med} ($\times10^{-6}$ mm^2/s)	1062.61 (714.00–1367.13)
P10ADC ($\times10^{-6}$ mm^2/s)	781.01 (373.85–1096.76)
P25ADC ($\times10^{-6}$ mm^2/s)	911.53 (598.74–1171.70)
P50ADC ($\times10^{-6}$ mm^2/s)	1050.22 (716.27–1366.78)
P75ADC ($\times10^{-6}$ mm^2/s)	1242.01 (849.79–1695.77)
P90ADC ($\times10^{-6}$ mm^2/s)	1445.89 (1006.36–2012.35)
Skewness	0.97 (0.19–2.22)
Kurtosis	2.09 (-0.49–7.10)
Entropy	6.75 (5.94–7.30)
D histogram parameters	
D_{min} ($\times10^{-6}$ mm^2/s)	400.50 (203.00–734.00)
D_{max} ($\times10^{-6}$ mm^2/s)	1855.00 (1206.00–3267.00)
D_{mean} ($\times10^{-6}$ mm^2/s)	867.78 (627.07–1156.55)
D_{med} ($\times10^{-6}$ mm^2/s)	827.94 (609.54–1128.10)
P10D ($\times10^{-6}$ mm^2/s)	639.04 (403.71–851.35)
P25D ($\times10^{-6}$ mm^2/s)	716.20 (529.21–976.90)
P50D ($\times10^{-6}$ mm^2/s)	825.68 (607.31–1129.16)
P75D ($\times10^{-6}$ mm^2/s)	982.17 (715.06–1421.78)
P90D ($\times10^{-6}$ mm^2/s)	1127.27 (827.10–1744.78)
Skewness	1.08 (0.84–2.14)
Kurtosis	2.29 (-1.30–9.64)
Entropy	6.70 (5.77–7.21)
F histogram parameters	
F_{min} (%)	0
F_{max} (%)	100
F_{mean} (%)	17.26 (11.30–29.61)
F_{med} (%)	14.54 (8.86–21.66)
P10F (%)	6.08 (0.14–11.55)
P25F (%)	8.88 (0.35–15.09)
P50F (%)	13.66 (8.64–19.38)
P75F (%)	18.84 (13.14–26.45)
P90F (%)	27.26 (19.50–38.11)
Skewness	2.95 (0.38–5.01)
Kurtosis	10.45 (-0.39–42.79)
Entropy	6.39 (5.69–7.20)

The data are expressed as median (range).
SUV, maximum standardized uptake value, MTV, metabolic tumour volume, TLG, total lesion glycolysis, ADC, apparent diffusion coefficient, D, slow diffusion coefficient, F, perfusion-related diffusion fraction, PnADC, the nth percentile of ADC, PnD, the nth percentile of D, PnF, the nth percentile of F.

Comparative analysis of the clinicopathological features

Electronic Supplementary Material Table S1 shows the comparison between the PET parameters and histogram parameters of ADC, D, and F between subgroups of tumour size, FIGO stage, SCC-ag level and grades. MTV ($p<0.001$), TLG ($p<0.001$), skewnessADC ($p=0.025$), kurtosisADC ($p=0.001$), entropy ADC ($p=0.003$), and kurtosisD ($p=0.013$)

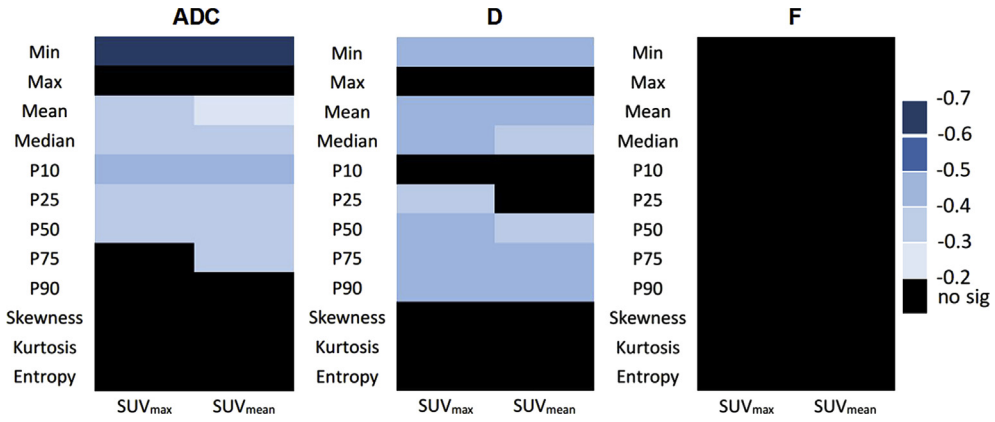

Figure 2 Matrix plot demonstrating the significant correlation coefficients between SUV and histogram parameters of ADC, D, and F of primary CSCC. Blue entries of diverse levels indicate significant negative correlations. Spearman's correlation coefficient (R) (see colour scale). Black entries indicate no significant correlations. SUV, standardized uptake value, ADC, apparent diffusion coefficient, D, slow diffusion coefficient, F, perfusion-related diffusion fraction, Pn, the nth percentile.

were significantly higher in tumour with larger diameters. In FIGO stage subgroups, MTV (p=0.007), TLG (p=0.010), skewnessF (p=0.014), and kurtosisF (p=0.034) were significantly higher in advanced-stage tumours. MTV (p=0.024), TLG (p=0.029), kurtosisADC (p=0.005) and entropyADC (p=0.012) were significantly higher with SCC-ag levels ≥4 ng/ml than with SCC-ag levels <4 ng/ml. Regarding tumour grades, MTV (p=0.003), TLG (p=0.004), and P75F (p=0.014) were significantly higher in G3 tumours than in G1/2 tumours, whereas P10ADC (p=0.001), P25ADC (p=0.021), and P10D (p<0.001) were significantly lower in G3 tumours. The ROC analysis (Fig 3 and Table 3) indicates that P10D accounted for the highest AUC (0.868), with a cut-off value of 592.28×10^{-6} mm2/s and a sensitivity and specificity of 92.31% and 80.65%, PPV and NPV of 66.68% and 96.15%, respectively. Detailed results of the other parameters are presented in Table 3.

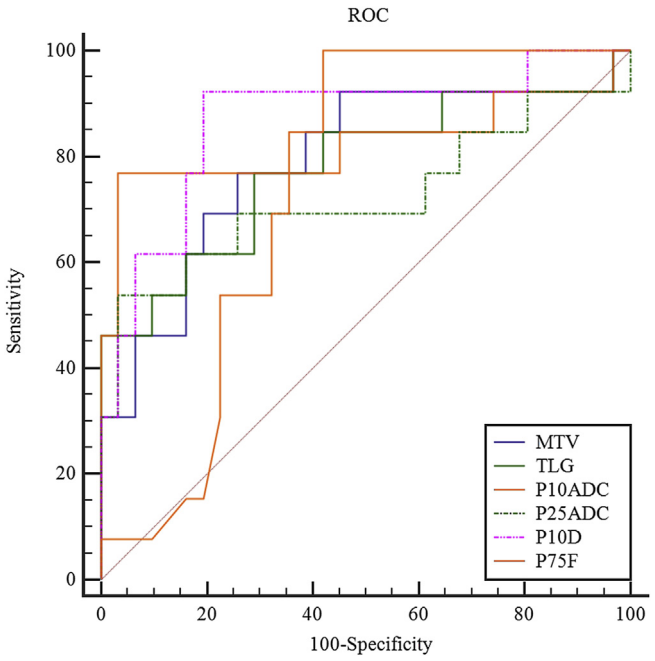

Figure 3 ROC analysis of PET and histogram parameters of ADC, D, and F in distinguishing G3 from G1/2 cervical squamous cell cancer. ROC, receiver operator characteristic curve, MTV, metabolic tumour volume, TLG, total lesion glycolysis, ADC, apparent diffusion coefficient, D, slow diffusion coefficient, F, perfusion-related diffusion fraction, PnADC, the nth percentile of ADC, PnD, the nth percentile of D, PnF, the nth percentile of F.

Discussion

The present study demonstrates that SUV and histogram parameters of ADC, D, and F were only very weakly correlated or not correlated at all, except for a moderately significant negative correlation between SUV and ADC_{min}. Among all the parameters, MTV, TLG, and IVIM histogram heterogeneity parameters were more related to tumour size, stage, and SCC-ag levels, while the 10th percentile of D performed better in distinguishing tumour grades.

Previous investigative results of the correlation between PET and DWI parameters in cervical cancer have not been consistent.[3,19–23] The moderate negative correlation between SUV_{max} and ADC_{min} obtained in the present study was consistent with results of Nakamura *et al.*,[3] Grueneisen *et al.*,[20] and Brandmaier *et al.*,[22] representing the consistency of the maximum tumour glucose metabolism activity and maximum cell density, but the correlation between SUV and IVIM histogram parameters has rarely been observed. This finding may be attributed to the tumour internal heterogeneity as prolonged growth, which is more likely to include normal tissue, vasculature, inflammatory reaction zones and necrotic zones, thereby weakening the negative correlation. We noticed that SUV_{max} had the strongest correlation with ADC_{min} in all parameters (r=-0.69, p<0.001). As a parameter used to characterize pure extravascular molecular diffusion, there was only a weak correlation between D_{min} and SUV_{max} or SUV_{mean}. Lee *et al.*[24] found that cervical cancer have low diffusion and low perfusion IVIM characteristics, supporting the notion that perfusion contributes to ADC.

Table 3
Cut-off values and diagnostic abilities of imaging parameters for distinguishing G3 from G1/2 cervical squamous cell cancer.

	Cut-off value	Sensitivity (%)	Specificity (%)	PPV (%)	NPV (%)	AUC
MTV (ml)	29.70	76.92	74.19	55.56	88.46	0.792
TLG (g)	255.47	76.92	70.97	52.64	88.00	0.779
P10ADC ($\times10^{-6}$ mm^2/s)	665.80	76.92	96.77	90.90	90.91	0.824
P25ADC ($\times10^{-6}$ mm^2/s)	734.33	53.85	96.77	87.49	83.33	0.722
P10D ($\times10^{-6}$ mm^2/s)	592.28	92.31	80.65	66.68	96.15	0.868
P75F ($\times$100%)	17.96	100	59.06	50.61	100	0.737

MTV, metabolic tumour volume, TLG, total lesion glycolysis, ADC, apparent diffusion coefficient, D, slow diffusion coefficient, F, perfusion-related diffusion fraction, PnADC, the nth percentile of ADC, PnD, the nth percentile of D, PnF, the nth percentile of F, PPV, positive predictive value, NPV, negative predictive value, AUC, area under curve.

The perfusion parameter F provided by the IVIM model is also meaningful, showing great efficiency in predicting treatment responses.[12,13] Dynamic contrast-enhanced MRI (DCE-MRI) parameters have been more frequently used to describe tumour perfusion. Some studies of cervical cancer[25,26] have shown positive correlations between IVIM perfusion parameters and DCE-MRI perfusion parameters. If IVIM imaging can replace DWI and DCE-MRI in certain conditions while simultaneously providing water molecule diffusion and perfusion information, it will reduce the use of contrast agents and enhance patient comfort. The correlation of SUV and F histogram parameters did not reach statistical significance in the present study. At first, this may have been because perfusion may contribute little to the entire diffusion effect, with an average of 14.9±2.6% in the study of Lee *et al.*[24] and a median of 17.26% in the present study. Then, F mainly represents microcirculatory perfusion, depending on various factors and the interactions of the tumour complex microenvironment, which is more complex than the DCE-MRI parameters. Finally, perfusion parameters are known to be more prone to measurement errors and rely on signal-to-noise ratios,[27] suggesting that voxel-by-voxel analysis may not be suitable for perfusion parameters. The present findings were consistent with those of Song *et al.*,[28] who found that the reproducibility of the F and D* histograms was poorer than that of ADC and D. D* map analysis was excluded, but the F map was included because it does not have as much noise as the D* map, and the extreme points in the histogram are on both sides; thus, these points did not overly influence the overall distribution, except for the maximum and minimum values.

In addition to SUV, volume-based PET metabolic parameters (MTV and TLG) also proved to evaluate clinicopathological features and predict prognosis.[5,6,14] Unsurprisingly, strong volume concordance between ^{18}F-FDG PET and T2WI[21] makes for larger masses having high MTV and TLG values. Previous studies[3,29] showed that SUV_{max} was significantly different between subgroups based on tumour size, a difference that was not significant in the present study. Additionally, large tumours have high histogram heterogeneity parameters, which is a manifestation of tumour invasion and internal heterogeneity enhancement. FIGO stages are crucial for precisely assessing prognostic factors and for determining the optimal treatment. Nakamura *et al.*[3] found that SUV_{max} was significantly different in early and advanced FIGO stages, but Pan *et al.*[29] did not find this. MTV and TLG were not assessed in these two studies; however, in a retrospective analysis of 49 patients with primary cervical cancer,[14] SUV_{max}, MTV, and TLG were found to differ significantly between FIGO stage Ib–IIa and IIb–IVb. Literature on the correlation between PET parameters and clinicopathological features of cervical cancer[3,14,29] including the present research rarely took the correction of surrounding background tissue into consideration. SUV tends to be affected by many factors, including time after injection, thus the correlation between SUV and tumour characteristics varied. The $SUV_{max/mean}$ results were not useful in the present research as delayed intake weakened the difference among each $SUV_{max/mean}$. Nevertheless, MTV or TLG, when combined with relative glucose metabolism and tumour volume, can better characterize clinicopathological features. Compared with PET parameters, ADC are more controversial in distinguishing different FIGO stages. The ADC_{mean} has the ability to distinguish early and advanced FIGO stages, as reported by Miccò *et al.*,[14] but the ADC_{min} was not shown to have this ability in another study.[3] IVIM histogram analysis was used to further confirm that F histogram heterogeneity parameters (skewnessF and kurtosisF) are useful for FIGO stage discrimination. SCC-ag is another important clinical indicator of preoperative predictions of survival outcomes and recurrence.[29] Similar to the present study, some studies have found that MTV and TLG were related to preoperative SCC-ag levels[4] and SUV_{max} was not.[29] In addition, the present study found unprecedentedly that ADC histogram heterogeneity parameters (kurtosisADC and entropyADC) are also related to SCC-ag levels.

Regarding the assessment of tumour grade, Grueneisen *et al.*[30] showed that G3 tumours had significantly higher SUV_{max} and SUV_{mean} and lower ADC_{min}, but Miccò *et al.*[14] did not find significant differences in ADC_{mean}, SUV_{max}, or even MTV and TLG. The present study demonstrated a deviation in MTV and TLG in differentiating tumour grades, which may have been because most of the G3 patients had large-sized tumours, resulting in a significant increase in MTV and TLG. In the ADC histogram analysis, Xue *et al.*[31] found that histogram-based ADC values were helpful in differentiating pathological types of cervical cancer, and low percentile values (P5ADC) had the largest AUC (0.83) in distinguishing well/moderately from poorly differentiated tumours. Lower ADC or D percentile values can detect higher cellular regions sensitively,[32] and higher ADC or D

percentile values have been shown to reflect low intracellular areas of tumours, such as necrotic or cystic regions.[27] The present study further confirmed the IVIM histogram analysis approach as a promising tool in discriminating tumour grades, and the low D percentile (P10D) has substantial diagnostic ability. The better diagnostic performance of P10D for tumour grades in the present study benefited from a PET-derived whole-tumour ROI measurement and the usage of bi-exponential curve-fitting metrics. Manual adjustment of the ROIs of the ADC maps with reference to the PET image in the present study can more accurately exclude the relatively free diffusion than just referring to the T1WI or T2WI in the other IVIM studies,[15,17,18,31] but the influence of inaccurate delineation was not the main focus of the present study. P75F was also proved to distinguish G3 tumours from G1/2 tumours in the present study. Cervical cancer exhibits the characteristic of low perfusion,[24] resulting from the relatively rapid decrease in microvessel density due to the excessive growth of central tumour regions. Zhou *et al.*[25] found that the difference in F values between high- and low-grade cervical cancer was affected by the location of the ROI. The F value in a peripheral ROI of G1/2 tumours was lower than that in G3 tumours. For the whole-tumour ROI, the F value of G1 tumours was higher than that of G3 tumours. P75F consists of higher F percentiles, representing the peripheral area of a tumour, so P75F in G3 tumours is higher than in G1/2 tumours. The present study further confirmed the results of Zhou *et al.*[25] The blood supply variation in the tumour centre, represented by low F percentile values, was greater, and the peripheral area of the tumour more closely reflected tumour characteristics; however, this histogram analysis of F maps is not recommended until the image quality is improved.

This study also had several limitations. Firstly, the sample size in the present study was small. Only two patients had metastatic lymph nodes confirmed by postoperative histopathology, and the cervical stromal invasion depth of all lesions in the surgical group was >50%, so those characteristics could not be analysed. Secondly, patients with lesions <2 cm were excluded; however, future improvements in PET and MRI equipment and techniques can allow improved spatial resolution to accurately assess small lesions. Thirdly, approximately 40 parameters were tested to find meaningful biomarkers comprehensively, but no multivariant analysis was performed or any method was applied to adjust for multiple testing. The reason was that it would not be convincing to do multivariant analysis or adjustment for multiple testing based on such a relatively small number of patients and large number of parameters in this study. This will be implemented in future research through incorporating larger patient cohorts and more comprehensive parameters. Haemorrhagic/cystic/necrotic tumour components or the endocervical canal of PET images and ADC maps were manually adjusted without limiting the parameter range to exclude some of the extreme values. Finally, due to the continuous uptake of the tumours, the delayed PET/MRI had an impact on the absolute distribution of SUV, which may be the reason why significant differences were not found in the clinicopathological features.

In conclusion, this clinical study demonstrates no universal correlations between SUV and IVIM parameters, and further investigation of PET and IVIM parameters, such as MTV, TLG, and IVIM histogram parameters, as independent potential biomarkers would be applied for evaluating clinicopathological characteristics of cervical cancer. In all, integrated PET/MRI has huge application potential in tumour with multi-parameter by multi-method imaging.

Conflicts of interest

None declared.

Acknowledgements

The authors thank Dr Qijun Wu for his constructive advice on the statistical analysis. This work was supported by the National Natural Science Foundation of China (grant number 81401438), LIAONING Science & Technology Project (grant number 2017225012), and the National Key Research and Development Program of China (grant number 2016YFC0107102).

Appendix A. Supplementary data

Supplementary data to this article can be found online at https://doi.org/10.1016/j.crad.2018.11.003.

References

1. Torre LA, Bray F, Siegel RL, *et al*. Global cancer statistics, 2012. *CA Cancer J Clin* 2015;**65**(2):87–108.
2. Onal C, Reyhan M, Parlak C, *et al*. Prognostic value of pretreatment ^{18}F-fluorodeoxyglucose uptake in patients with cervical cancertreated with definitive chemoradiotherapy. *Int J Gynecol Cancer* 2013;**23**(6):1104–10.
3. Nakamura K, Joja I, Kodama J, *et al*. Measurement of SUVmax plus ADCmin of the primary tumour is a predictor of prognosis in patients with cervical cancer. *Eur J Nucl Med Mol Imag* 2012;**39**(2):283–90.
4. Xu W, Yu S, Xin J, *et al*. Relationship of ^{18}F-FDG PET/CT metabolic, clinical and pathological characteristics of primary squamous cell carcinoma of the cervix. *J Investig Med* 2016;**64**(8):1246–51.
5. Chung HH, Kim JW, Han KH, *et al*. Prognostic value of metabolic tumor volume measured by FDG-PET/CT in patients with cervical cancer. *Gynecol Oncol* 2011;**120**(2):270–4.
6. Crivellaro C, Signorelli M, Guerra L, *et al*. ^{18}F-FDG PET/CT can predict nodal metastases but not recurrence in early stage uterine cervical cancer. *Gynecol Oncol* 2012;**127**(1):131–5.
7. Kuang F, Ren J, Zhong Q, *et al*. The value of apparent diffusion coefficient in the assessment of cervical cancer. *Eur Radiol* 2013;**23**(4):1050–8.
8. Somoye G, Harry V, Semple S, *et al*. Early diffusion weighted magnetic resonance imaging can predict survival in women with locally advanced cancer of the cervix treated with combined chemo-radiation. *Eur Radiol* 2012;**22**(11):2319–27.
9. Makino H, Kato H, Furui T, *et al*. Predictive value of diffusion-weighted magnetic resonance imaging during chemoradiotherapy for uterine cervical cancer. *J Obstet Gynaecol Res* 2014;**40**(4):1098–104.
10. Le Bihan D, Breton E, Lallemand D, *et al*. Separation of diffusion and perfusion in intravoxel incoherent motion MRI imaging. *Radiology* 1988;**168**(2):497–505.

11. Chandarana H, Lee VS, Hecht E, *et al*. Comparison of biexponential and monoexponential model of diffusion weighted imaging in evaluation of renal lesions preliminary experience. *Invest Radiol* 2011;**46**(5):285–91.
12. Zhu L, Zhu L, Shi H, *et al*. Evaluating early response of cervical cancer under concurrent chemo-radiotherapy by intravoxel incoherent motion MRI imaging. *BMC Cancer* 2016;**16**:79.
13. Zhu L, Zhu L, Wang H, *et al*. Predicting and early monitoring treatment efficiency of cervical cancer under concurrent chemoradiotherapy by intravoxel incoherent motion magnetic resonance imaging. *J Comput Assist Tomogr* 2017;**41**(3):422–9.
14. Miccò M, Vargas HA, Burger IA, *et al*. Combined pre-treatment MRI and ^{18}F-FDG PET/CT parameters as prognostic biomarkers in patients with cervical cancer. *Eur J Radiol* 2014;**83**(7):1169–76.
15. Downey K, Riches SF, Morgan VA, *et al*. Relationship between imaging biomarkers of stage I cervical cancer and poor-prognosis histologic features: quantitative histogram analysis of diffusion-weighted MRI images. *AJR Am J Roentgenol* 2013;**200**(2):314–20.
16. Nougaret S, Vargas HA, Lakhman Y, *et al*. Intravoxel incoherent motion-derived histogram metrics for assessment of response after combined chemotherapy and radiation therapy in rectal cancer: initial experience and comparison between single-section and volumetric analyses. *Radiology* 2016;**280**(2):446–54.
17. Erbay G, Onal C, Karadeli E, *et al*. Predicting tumor recurrence in patients with cervical carcinoma treated with definitive chemoradiotherapy: value of quantitative histogram analysis on diffusion-weighted MRI images. *Acta Radiol* 2017;**58**(4):481–8.
18. Lin Y, Li H, Chen Z, *et al*. Correlation of histogram analysis of apparent diffusion coeffcient with uterine cervical pathologic finding. *AJR Am J Roentgenol* 2015;**204**(5):1125–31.
19. Ho KC, Lin G, Wang JJ, *et al*. Correlation of apparent diffusion coefficients measured by 3 T diffusion-weighted MRI and SUV from FDG PET/CT in primary cervical cancer. *Eur J Nucl Med Mol Imag* 2009;**36**(2):200–8.
20. Grueneisen J, Beiderwellen K, Heusch P, *et al*. Correlation of standardized uptake value and apparent diffusion coefficient in integrated whole-Body PET/MRI of primary and recurrent cervical cancer. *PLoS One* 2014;**9**(5):e96751.
21. Sun H, Xin J, Zhang S, *et al*. Anatomical and functional volume concordance between FDG PET, and T2 and diffusion weighted MRI for cervical cancer: a hybrid PET/MRI study. *Eur J Nucl Med Mol Imag* 2014;**41**(5):898–905.
22. Brandmaier P, Purz S, Bremicker K, *et al*. Simultaneous ^{18}F-FDG-PET/MRI: correlation of apparent diffusion coefficient (ADC) and standardized uptake value (SUV) in primary and recurrent cervical cancer. *PLoS One* 2015;**10**(11):e0141684.
23. Surov A, Meyer HJ, Schob S, *et al*. Parameters of simultaneous ^{18}F-FDG-PET/MRI predict tumor stage and several histopathological features in uterine cervical cancer. *Oncotarget* 2017;**8**(17):28285–96.
24. Lee EY, Yu X, Chu MM, *et al*. Perfusion and diffusion characteristics of cervical cancer based on intraxovel incoherent motion MRI imaging-a pilot study. *Eur Radiol* 2014;**24**(7):1506–13.
25. Zhou Y, Liu J, Liu C, *et al*. Intravoxel incoherent motion diffusion weighted MRI of cervical cancer correlated with tumor differentiation and perfusion. *Magn Reson Imag* 2016;**34**(8):1050–6.
26. Lee EY, Hui ES, Chan KK, *et al*. Relationship between intravoxel incoherent motion diffusion-weighted MRI and dynamic contrast-enhanced MRI in tissue perfusion of cervical cancers. *J Magn Reson Imag* 2015;**42**(2):454–9.
27. Koh DM, Collins DJ, Orton MR. Intravoxel incoherent motion in body diffusion-weighted MRI: reality and challenges. *AJR Am J Roentgenol* 2011;**196**(6):1351–61.
28. Song YS, Park CM, Lee SM, *et al*. Reproducibility of histogram and texture parameters derived from intravoxel incoherent motion diffusion-weighted MRI of FN13762 rat breast carcinomas. *Anticancer Res* 2014;**34**(5):2135–44.
29. Pan L, Cheng J, Zhou M, *et al*. The SUV_{max} (maximum standardized uptake value for f-18 fluorodeoxyglucose) and serum squamous cell carcinoma antigen (scc-ag) function as prognostic biomarkers in patients with primary cervical cancer. *J Cancer Res Clin Oncol* 2012;**138**(2):239–46.
30. Grueneisen J, Schaarschmidt BM, Heubner M, *et al*. Integrated PET/MRI for whole-body staging of patients with primary cervical cancer: preliminary results. *Eur J Nucl Med Mol Imag* 2015;**42**(12):1814–24.
31. Xue HD, Ren C, Yang JX, *et al*. Histogram analysis of apparent diffusion coefficient for the assessment of local aggressiveness of cervical cancer. *Arch Gynecol Obste* 2014;**290**(2):341–8.
32. Song YS, Choi SH, Park CK, *et al*. True progression versus pseudoprogression in the treatment of glioblastomas: a comparison study of normalized cerebral blood volume and apparent diffusion coefficient by histogram analysis. *Kor J Radiol* 2013;**14**(4):662–72.